DEPARTMENT OF MECHANICAL ENGINEERING AND MECHANICS
COLLEGE OF ENGINEERING
OLD DOMINION UNIVERSITY
NORFOLK, VIRGINIA 23508

NUMERICAL SOLUTIONS OF NAVIER-STOKES EQUATIONS FOR A BUTLER WING

By

Jamshid S. Abolhassani

and

Surendra N. Tiwari, Principal Investigator

Final Report
For the period January 1, 1986 to January 1, 1987

Prepared for the
National Aeronautics and Space Administration
Langley Research Center
Hampton, VA 23665

Under
Research Grant NCC1-68
Dr. Robert E. Smith, Jr. Technical Monitor
ACD-Computer Applications Branch

January 1987

DEPARTMENT OF MECHANICAL ENGINEERING AND MECHANICS
COLLEGE OF ENGINEERING
OLD DOMINION UNIVERSITY
NORFOLK, VIRGINIA 23508

NUMERICAL SOLUTIONS OF NAVIER-STOKES EQUATIONS FOR A BUTLER WING

By

Jamshid S. Abolhassani

and

Surendra N. Tiwari, Principal Investigator

Final Report
For the period January 1, 1986 to January 1, 1987

Prepared for the
National Aeronautics and Space Administration
Langley Research Center
Hampton, VA 23665

Under
Research Grant NCC1-68
Dr. Robert E. Smith, Jr. Technical Monitor
ACD-Computer Applications Branch

Submitted by the
Old Dominion University Research Foundation
P.O. Box 6369
Norfolk, Virginia 23508

January 1987

TABLE OF CONTENTS

	Page
Abstract	iii
Nomenclature	iv
Introduction	1
Governing Equations	3
Method of Solution	8
Initial and Boundary Conditions	10
Applications to a Butler Wing	13
Results and Discussion	14
Concluding Remarks	18
Acknowledgement	19
References	20

LIST OF FIGURES

Figure		Page
1	Physical Model of a Butler Wing	21
2	H-Type Grid for a Butler Wing	21
3a	Pressure Coefficient Along the Center Line	22
3b	Pressure Ratio at 41.67% of Chord	22
3c	Pressure Ratio at 68.33% of Chord	22
4	O-Type Grid for a Butler Wing	22
5a	Pressure Coefficient Along the Center Line	23
5b	Pressure Ratio at 41.67% of Chord	23
5c	Pressure Ratio at 68.33% of Chord	23
5d	Cross-flow velocity vectors (Zero Angle of Attack)	23
6a	Pressure Coefficient (X/C 17%, Ten Degree Angle of Attack)	24

TABLE OF CONTENTS - Continued

LIST OF FIGURES - Continued

Figure		Page
6b	Pressure Coefficient (X/C 30%, Ten Degree Angle of Attack)	24
6c	Pressure Coefficient (X/C 50%, Ten Degree Angle of Attack)	24
6d	Pressure Coefficient (X/C 70%, Ten Degree Angle of Attack)	24
6e	Pressure Coefficient (X/C Ten Degree Angle of Attack	25

NUMERICAL SOLUTIONS OF NAVIER-STOKES EQUATIONS FOR A BUTLER WING

Jamshid S. Abolhassani [1]

Surendra N. Tiwari [2]

Abstract

The flow field is simulated on the surface of a Butler wing in a uniform stream. Results are presented for Mach number 3.5 and Reynolds number of 2,000,000. The simulation is done by integrating the viscous Navier-Stokes equations. These equations govern the unsteady, viscous, compressible and heat conducting flow of an ideal gas. The equations are written in curvilinear coordinates so that the wing surface is represented accurately. O-type and H-type grids have been used for this study, and results are compared. The governing equations are solved by the MacCormack time-split method, and the results are compared with other theoretical and experimental results. The codes are written in FORTRAN, vectorized and currently run on the CDC Vector Processing System (VPS-32) computer.

---

[1] Graduate Research Assistant, Department of Mechanical Engineering and Mechanics, Old Dominion University, Norfolk, Va, 23508, AIAA Student Member.

[2] Eminent Professor, Department of Mechanical Engineering and Mechanics, Old Dominion University, Norfolk, VA, 23508, AIAA Associate Fellow.

Nomenclature

C_v	specific heat at constant volume
e	internal energy per unit volume
E	total energy per unit volume
$\bar{F}$, $\bar{G}$, $\bar{H}$	vector fluxes for coordinates directions
J	Jacobin matrix
κ	coefficient of bulk viscosity
K	coefficient of thermal conductivity
L	length of the wing
M	Mach number
n	magnitude of normal vector on any surface
P	static pressure
p_r	prandtl number
q_x, q_y, q_z	components of heat conduct vectors
R	universal gas constant
R_e	Reynolds number
T	static temperature
T_∞	free stream temperature
T_w	wall temperature
T_r	reference temperature for Sutherland viscosity law
t	time
S_o	constant for Sutherland viscosity law
$\bar{U}$	vector of state variables
u,v,w	velocity components in the physical coordinates
V_ℓ	contravariant velocity in the computational coordinates
x,y,z	coordinates for the physical domain
α	coefficient for pressure damping

γ	ratio of specific heat
ξ,η,ζ	coordinates for the computational domain
μ	molecular viscosity
μ_r	reference viscosity in Sutherland viscosity law
μ'	bulk viscosity
ρ	density
τ	stress tensor
$\tau_{xx},\tau_{xy},\tau_{xz}$	elements of the stress tensor
$\tau_{yy},\tau_{yz},\tau_{zz}$	components of viscous dissipation functions
$\phi_x,\phi_y,\phi_z,\ \delta_{ij}$	Kronecker delta function

subscript

w	solid walls
∞	free stream value

superscript

n	time level

indices

i,j,k	point indices

operators

∇	gradient
o	inner product
$L\xi,L\eta,L\zeta$	finite difference operators
∂	partial differentiations

Introduction

The Butler wing is a delta wing which was proposed by D. S. Butler 1. The planform of the body is an isosceles triangle, and the leading edges of the wing lay along the Mach lines of the unperturbed stream. The first 20% of the wing is conical and the last 80% of the wing has elliptical cross sections with increasing eccentricity along the x-axis. At the trailing edge, the elliptical cross section has infinite eccentricity and this last cross section is a straight line. D. S. Butler has compared the experimental results for surface pressure with the theoretical results using the slender-body theory approximation to simplify the inviscid equations of motion[1]. Walkden and Caine estimated the pressure on the surface of a Butler wing at zero incident in a steady uniform stream by numerically integrating the two semi-characteristic forms of the equations governing inviscid supersonic flow of an ideal gas with constant specific heat[2]. Squire obtained experimental results for a Butler wing varying Mach number and angle of attack[3]. Inviscid equations have been used in all previous analytical and numerical investigations.

In order to study the flow around a Butler wing, the Navier-Stokes equations are numerically solved. The equations are unsteady, compressible, viscous and three-dimensional. The time dependency of the governing equations allows the solution to progress naturally from an arbitrary initial guess to an asymptotic steady state, if one exists. The equations are transformed from physical coordinates to computational coordinates which allows solutions to be computed in a rectangular domain. The equations are solved by the MacCormack time-split technique[4, 5] which is vectorized and programmed to run on the CDC VPS-32 (CYBER 205) computer. The codes are written in 32-bit (half-word) FORTRAN.

The Butler wing is symmetric about (x-z) and (x-y) planes. This permits the use of one quarter of the entire physical domain for flow field computation with zero angle of attack (Fig. 1). However, if the angle of attack is greater than zero, then half of the physical domain should be considered.

Grid generation is the first step which should be considered in obtaining flow field solutions over any configuration. Due to the data base management of the present program, it is necessary to map entire physical domain into a rectangular parallelepiped. Among the grid types, selection of an O-type grid for cross sections in the x-coordinate direction would produce a point singularity at the nose tip and a line singularity along the trailing edges. Nevertheless, an O-type grid maps the solid boundary onto an entire face of the parallelepiped. It is also possible to generate a highly orthogonal grid in the regions where there are relative high curvatures. However, a H-type grid does not map the solid boundary onto an entire face of the computational box. This creates a potential problem in updating the boundary conditions near the leading edges of the wing and also the grid in some regions could be highly skewed. But, there are no singularities in the grid. Both types of grid have been used in this study, and results are compared with other numerical, analytical and experimental results.

Governing Equations

The governing equations for a thermal fluid system are the conservation of mass, momentum and energy. These equations are developed for an arbitrary region under the assumption that the system is a continuum. Equations of motion for viscous, compressible, unsteady and heat conducting flow can be written as:

Continuity: $$\frac{\partial \rho}{\partial t} + \nabla\cdot(\rho\bar{u}) = 0, \tag{1a}$$

Momentum: $$\frac{\partial(\rho\bar{u})}{\partial t} + \nabla\cdot(\rho\bar{u}\bar{u} - \bar{\bar{\tau}}) = 0, \tag{1b}$$

Energy: $$\frac{\partial E}{\partial t} + \nabla\cdot(E\bar{u} + \bar{\dot{q}} - \bar{u}\cdot\bar{\bar{\tau}}) = 0, \tag{1c}$$

where E is the total energy per unit volume given by $E = \rho\,(e + u\cdot u/2)$ and e is the internal energy per unit volume. Equations 1b and 1c can be simplified by assuming that the stress at a point is linearly dependent on the rate of strain (deformation) of the fluid (Newtonian fluid),

$$\tau_{ij} = -\,p\delta_{ij} + \mu\left(\frac{\partial u_i}{\partial x_j} + \frac{\partial u_j}{\partial x_i}\right) + \delta_{ij}\,\mu'\,\frac{\partial u_k}{\partial x_k}, \tag{2a}$$

where δ_{ij} is Kronecker delta function, and μ' is the second coefficient of viscosity which is related to the coefficient of bulk viscosity (κ) by the expression $\kappa = 2\,\mu/3 + \mu'$. The contribution of κ can be neglected if the pressure in a fluid is not changed abruptly during its expansion or contraction. Under this assumption, the stress tensor can be related to the pressure and velocity components as:

$$\tau_{ij} = -\,p\delta_{ij} + \mu\left[\left(\frac{\partial u_i}{\partial x_j} + \frac{\partial u_j}{\partial x_i}\right) - \frac{2}{3}\,\delta_{ij}\,\frac{\partial u_k}{\partial x_k}\right]. \tag{2b}$$

For an isotropic system, the heat flux in Eq. (1c) can be expressed in terms of temperature gradient (Fourier law of heat conduction) as:

$$\bar{\dot{q}} = - K\nabla T \tag{3}$$

where K is the coefficient of thermal conductivity. A common approximation used for viscosity is based on the kinetic theory of gases using an idealized intermolecular-forces potential; the relation is

$$\frac{\mu}{\mu_r} = \left(\frac{T}{T_r}\right)^{3/2} \frac{T_r + S_o}{T + S_o} \tag{4}$$

where

$$S_o = 198^{\circ}R;$$

$$\mu_r = 0.1716 \text{ np}$$

The coefficients of thermal conductivity K can be determined from Prandtl number as

$$K = \frac{\gamma \mu C_v}{P_r}, \tag{5}$$

where C_v is the specific heat at constant volume and γ is the ratio of specific heats.

It is essential to have a supplementary relation to close the system of equations (1a-1c). By neglecting the inter-molecular forces (thermally perfect system), thermodynamic properties can be described as:

$$p = \rho RT, \tag{6}$$

where R is the universal gas constant. Thermally perfect gas assumption permits to express the internal energy as a function of temperature only i.e., e=e(T). In addition, assumption of calorically perfect gas [e(0)=0] allows the

following relation:

$$e = C_v T. \tag{7}$$

A substitution of Eq. (6) into Eq. (7) results in

$$p = \rho e (\gamma-1). \tag{8}$$

The equations of motion are in conservative form. For simplicity, these equations can be written in a compact vector form as

$$\frac{\partial U}{\partial t} + \frac{\partial F}{\partial x} + \frac{\partial G}{\partial y} + \frac{\partial H}{\partial z} = 0, \tag{9}$$

where

$$U = \begin{Bmatrix} \rho \\ \rho u \\ \rho v \\ \rho w \\ E \end{Bmatrix}, \quad F = \begin{Bmatrix} \rho u \\ \rho uu - \tau_{xx} + p \\ \rho uv - \tau_{xy} \\ \rho uw - \tau_{xz} \\ Eu + \dot{q}_x - \phi_x + pu \end{Bmatrix},$$

$$G = \begin{Bmatrix} \rho v \\ \rho uv - \tau_{yx} \\ \rho vv - \tau_{yy} + p \\ \rho vw - \tau_{yz} \\ Ev + \dot{q}_y - \phi_y + pv \end{Bmatrix}, \quad H = \begin{Bmatrix} \rho w \\ \rho uw - \tau_{zx} \\ \rho vw - \tau_{zy} \\ \rho ww - \tau_{zz} + p \\ Ew + \dot{q}_z - \phi_z + pw \end{Bmatrix}.$$

For the sake of generality, the governing equations are transformed from a physical domain into a computational domain as

$$\frac{\partial U}{\partial t} + \begin{Bmatrix} \xi_x \\ \xi_y \\ \xi_z \end{Bmatrix} \left(\frac{\partial F}{\partial \xi}, \frac{\partial G}{\partial \xi}, \frac{\partial H}{\partial \xi}\right) +$$

$$\begin{Bmatrix} \eta_x \\ \eta_y \\ \eta_z \end{Bmatrix} + \left(\frac{\partial F}{\partial \eta}, \frac{\partial G}{\partial \eta}, \frac{\partial H}{\partial \eta}\right) + \begin{Bmatrix} \zeta_x \\ \zeta_y \\ \zeta_z \end{Bmatrix} \left(\frac{\partial F}{\partial \zeta}, \frac{\partial G}{\partial \zeta}, \frac{\partial H}{\partial \zeta}\right) = 0. \tag{10}$$

The transformation coefficients can be computed from a functional relation between the computational coordinates and the physical coordinates.

$$\xi = \xi(x,y,z), \quad \eta = \eta(x,y,z), \quad \zeta = \zeta(x,y,z). \tag{11}$$

If Eq. (11) were known, the transformation coefficient could have be computed by direct differentiation. If not, after some algebraic manipulations, the transformation coefficients can computed by

$$\begin{aligned}
\xi_x &= (y_\eta z_\zeta - y_\zeta z_\eta) \,/\, |J^{-1}|, \\
\xi_y &= -(x_\eta z_\zeta - x_\zeta z_\eta) \,/\, |J^{-1}|, \\
\xi_z &= (x_\eta y_\zeta - x_\zeta y_\eta) \,/\, |J^{-1}|, \\
\eta_x &= -(y_\xi z_\zeta - y_\zeta z_\xi) \,/\, |J^{-1}|, \\
\eta_y &= (x_\xi z_\zeta - x_\zeta z_\xi) \,/\, |J^{-1}|, \\
\eta_z &= -(x_\xi y_\zeta - x_\zeta y_\xi) \,/\, |J^{-1}|, \\
\zeta x &= (y\xi \, z\eta - y\eta \, z\xi) \,/\, |J^{-1}|,
\end{aligned} \tag{12}$$

$$\zeta_y = -(x_\xi z_\eta - x_\eta z_\xi) \; / \; |J^{-1}|,$$

$$\zeta_z = (x_\xi y_\eta - x_\eta y_\xi) \; / \; |J^{-1}|,$$

where $[J^{-1}]$ is defined as

$$|J^{-1}| = x_\xi (y_\eta z_\zeta - y_\zeta z_\eta) - x_\eta (y_\xi z_\zeta - y_\zeta z_\xi)$$

$$+ x_\zeta (y_\xi z_\eta - y_\eta z_\xi). \qquad (13)$$

In the present case, the grid planes are perpendicular to the x-coordinate. Consequently, physical coordinates can be written as

$$x = x(\xi),$$

$$y = y(\xi,\eta,\zeta), \qquad (14)$$

$$z = z(\xi,\eta,\zeta).$$

This reduces the transformation coefficients from nine to five none zero elements therefore reducing the memory requirements.

Method of Solution

A time marching method is used to compute the solution so that the possible transient features can be readily captured. This method is an explicit second-order accurate time-split predictor-corrector algorithm [5]. The governing equation, Eq. (10) is discretized in computational directions. In a compact form, it can be expressed as

$$\bar{U}^{n+1}_{ijk} = [L_\eta(\Delta t_\eta)][L_\zeta(\Delta t_\zeta)][L_\xi(\Delta t_\xi)][L_\zeta(\Delta t_\zeta)][L_\eta(\Delta t_\eta)], \qquad (15)$$

where

$$\Delta t_\eta = \Delta t_\zeta = \frac{1}{2}\Delta t_\xi,$$

and L_ξ, L_η and L_ζ, are the operators in ξ, η and ζ directions, respectively. A time step is completed in this algorithm with the application of each operator applied symmetrically about the middle operator. For example, operator L_ξ can be defined as

$$L_\xi(\Delta t_\xi) = \bar{U}^{out}_{ijk}, \qquad (16)$$

for predictor step:

$$\bar{U}_{ijk} = \bar{U}^{in}_{ijk} - \frac{\Delta t_\xi}{\Delta\xi}[(\bar{F}_i - \bar{F}_{i-1})\frac{\partial\xi}{\partial x} + (\bar{G}_i - \bar{G}_{i-1})\frac{\partial\xi}{\partial y} + (\bar{H}_i - \bar{H}_{i-1})\frac{\partial\xi}{\partial z}]_{ijk} \qquad (17)$$

for corrector step:

$$\bar{U}^{out}_{ijk} = \frac{1}{2}[\bar{U}^{in}_{ijk} + \bar{U}_{ijk} - \frac{\Delta t_\xi}{\Delta\xi}[(\bar{F}_{i+1} - \bar{F}_i)\frac{\partial\zeta}{\partial x} + (\bar{G}_{i+1} - \bar{G}_i)\frac{\partial\xi}{\partial y} + (\bar{H}_{i+1} - \bar{H}_i)\frac{\partial\xi}{\partial z}]_{ijk}]. \qquad (18)$$

The solution is stable if the time step of each operator does not exceed the allowable step size for that operator. The finite difference scheme is consistent if the sum of the time steps for each operators are equal. The solution is second order accurate if operators are applied symmetrically.

This method has a time-step stability limit, but there is no rigorous stability analysis available. A commonly used conservative time-step is

$$\Delta t \leq \min \left[\frac{|u|}{\Delta x} + \frac{|v|}{\Delta y} + \frac{|w|}{\Delta z} + c\left(\frac{1}{\Delta x^2} + \frac{1}{\Delta y^2} + \frac{1}{\Delta z^2}\right)\right]^{-1}, \tag{19}$$

where c is the local speed of sound.

In the supersonic region, there exits a large gradient which requires a very fine mesh to resolve it. Most center difference methods admit a solution which has sawtooth or plus-minus waves with the shortest wave length that the mesh can support. In the case of a nonlinear problem, these short waves interact, vanish, and reappear again as distorted long waves or oscillations. These oscillations eventually blow up the solution,if they are not resolved. The oscillations of "low frequency" can be suppressed by adding a fourth order damping. A common damping used is the pressure dampening. This can be expressed in computational coordinates as

$$-\alpha_\ell \Delta t_\ell \delta_\ell^3 \frac{\partial}{\partial \delta_\ell} \frac{|V_\ell| + c}{4P} \frac{\partial^2 p}{\partial^2 \delta_\ell} \frac{\partial \bar{U}}{\partial \delta_\ell}, \quad \ell = 1,2,3 \tag{20}$$

where V_ℓ is the contravariant velocity.

Initial and Boundary Conditions

In computational fluid dynamics the initial conditions usually correspond to a real initial situation for a transient problem, or a rough guess for a steady state problem. In practice, initial conditions are obtained from experiments, empirical relations, approximate theories or previous computational results. An improper initial guess may result in generating unrealistic strong transient waves which propagate through the computational region dominating the flow field and eventually lead to a solution failure. An important requirement for the initial conditions is that they should be physically as close as possible to the actual nature of the flow field in the region under study. This will minimize the number of iterations required for convergence. An attractive approach is to initialize the entire flow field with a crude and simple guess (e.g., free stream condition). During the course of the computation, both body and upstream boundary conditions are changed in a gradual manner to their final values over a prescribed number of iterations. In the present study, this technique is applied in only one step which is equivalent to impulsive initial conditions.

It is equally important to implement a realistic, accurate and stable method to determine boundary conditions. The application of certain conditions may cause numerical instability even though the flow is physically stable. Most of the boundary conditions currently implemented are drawn mainly upon intuitions, simple analytical expressions, wind tunnel experiments and computational experimentations. In the selection of boundary conditions, consideration should be given to the following criteria: convergence, stability, computer time and above all the physical justification.

For the present case, there are five different boundary conditions. They are upstream, downstream, lateral, top, and solid boundary. For the case of H-

grid, the upstream boundary is located at six grid point spacings ahead of the nose of the wing. Following undisturbed free stream conditions are assumed for this boundary:

$$\bar{U}\Big|_{\text{upstream}} = \bar{U}_{\infty} \tag{21}$$

For the case of O-grid, the upstream boundary is set at 5% of the body length to avoid the singularities. The conical assumption has been made for this boundary[6]. Flow is said to be conical if the physical conditions such as pressure and velocity do not vary with position along any ray through a point, which is referred to as the vertex. For this case, the viscous-conical solutions are obtained for a cone at proper angle of attack. This is done by creating a conical grid, which is straight lines (rays) from the vertex and integrating the conical Navier-Stokes equations. This solution is valid provided the body is sufficiently slender.

A zero gradient in the y-direction (parallel to the primary direction of flow) is assumed for the downstream boundary, i.e.,

$$\frac{\partial \bar{U}}{\partial X}\Bigg| = 0. \tag{22}$$

The lateral boundaries are located far enough away form the body to avoid any influence on the interaction region. Presently, a zero gradient in the z-direction is assumed for these boundaries,i.e.,

$$\frac{\partial \bar{U}}{\partial z}\Bigg|_{\text{Top}} = 0. \tag{23}$$

The walls are assumed to be impermeable and no-slip boundary conditions are applied, therefore, all velocity components are assumed to be zero. Similarly, the wall is assumed to have a constant temperature T_w. A zero normal pressure gradient is assumed for the solid surface, i.e.,

$$\left.\frac{\partial P}{\partial n}\right|_{Solid} = 0. \tag{24}$$

This appears to be a boundary-layer approximation (i.e., a zero normal pressure gradient). It is, however, a much milder approximation, since constant pressure is not applied through the boundary layer but over one grid line in the boundary layer. This approximation has yielded stable computation for both the non-separated and separated boundary layers[7]. For general curviliear coordinates, Eq. (24) can be expressed as

$$\begin{aligned}
&(\xi_x\,\eta_x + \xi_y\,\eta_y + \xi_z\,\eta_z)\,P_\xi + \\
&(\eta^2{}_x + \eta^2{}_y + \eta^2{}_z)\,P_\eta + \\
&(\zeta_x\,\eta_x + \zeta_y\,\eta_y + \zeta_z\,\eta_z)\,P_\zeta = 0.
\end{aligned} \tag{25}$$

This equation is satisfactory even for skew grids near solid boundaries.

Applications to a Butler Wing

As mentioned in the introduction, the Butler wing is a delta wing which was proposed by D. S. Butler[1]. The Butler wing is analogous to an elliptic piston which the ratio of major and minor axes changes while disturbing the fluid. The plan form of the body (Fig. 1a) is an isosceles triangle, and leading edges of the wing are laid along the Mach lines of the undisturbed stream. For the first 20% of the length, the body is a right circular cone. The reminder of the body has elliptical sections which become more eccentric as the sharp trailing edges are approached (Fig. 1b). The semi major and minor axes are given by:

Major axis (semi-span) $= \frac{x}{\beta}$ (26a) $0<=x<=L$

Minor axis (thickness on centerline) $= \frac{x}{\beta}$ (26b) $0<=x<=0.2L$

$$= \frac{x}{\beta}\left[1 - \left(\frac{x- 0.2L}{0.8x}\right)^4\right] \quad (26c) \quad 0.2L<=x<=L$$

where $\beta^2 = M^2-1$

The model is 0.8 ft. (0.2438 m) long, and the geometry has been generated for Mach number of 3.5. That is the semi-apex angle of the plan form and the initial conical nose is $SIN^{-1}(1./3.5) = 16.602^{o}$.

This wing is symmetric about (xz) and (xy) planes. For zero angle of attack, this permits us to use only one quarter of the entire physical domain (Figs. 1a-1c) which is extremely advantageous from computational viewpoint. However, if the angle of attack is non-zero then half of the physical domain should be considered.

Some specific flow field results have been obtained for the Butler wing and these are discussed in the next section.

Results and Discussion

In the previous experiments[3], the surface oil-flow patterns over the wing at various angles of attack and at Mach number 3.5 showed no signs of transition and the nature of the oil streaklines was typical of a laminar flow. Therefore, results are obtained only for laminar flow over a Butler wing at Mach number of 3.5, Reynolds number of 2x106/ft (6.56x106/m), free static temperature of 390°R (216.67°K), wall temperature of 1092°R (606.67°K), length of 0.80 ft (0.2438 m), and at zero and ten degree angles of attack. In this study, a two boundary grid generation (TBGG) technique 4 is used, this method is essentially an algebraic method. The application of the TBGG method requires that the entire body be sliced into different cross-sections. These cross-sections are obtained in the stream-wise direction by analytical descriptions of the wing surface, (Eqs. 26a-26c). Then, two types of grid generated for this wing the H-type and O-type. Results of both cases are compared and discussed.

H-Type Grid

In this case, the entire flow field is sliced into fifty-five stations in the stream-wise direction, and each station has 64x36 grid points (Fig. 2). There is a total of 126,720 grid points which take 2.8 million 32-bit words of primary memory (16 variables). The required computational time is 1.9x10-5 sec/grid point/iteration (2.5 sec/iteration) which is typical for the CYBER 205 with two pipes. Results are obtained for zero angle of attack. The computed pressures are plotted in Figs. 3a-3c. The pressure coefficient along the center line is shown in Fig. 3a. The results are compared with available experimental and numerical results (Refs. 1,3,8). The results on the center line are in excellent agreement with the experimental and previously obtained

numerical results (Refs. 1,3,8). At 41.66% and 68.33% chordwise position, the pressure ratios are plotted against the conical spanwise coordinates y/xtan (ϕ), Figs. (3b and 3c). They are in good agreement with experimental and numerical results. However, There are some discrepancies in the results between 30° and 60°. This is probably due to the fact that grid lines are notorthogonal near those regions and is a direct consequence of the H-type grid.

O-Type Grid

For this case, the physical domain is limited to 5% to 95% of the wing. This is done to avoid any singularities. The conical Navier-Stokes solutions are forced for the upstream boundary which is located at 5% of the wing. This solution is obtained by the integration of the Navier-Stokes equations 6 for a conical grid with proper boundary conditions. The wing is sliced into forty-one stations in the stream-wise direction, and each station has 41x127 grid points (Fig 4). There is a total of 213,487 grid points which take 4.7 million 32-bit words of primary memory. Results are obtained for zero and ten degree angle of attack.

Results for zero angle of attack are compared with results obtained with the H-type grid, from the experiments and other numerical results (Refs. 1,3,8). The computed pressures are plotted in Figs. 5a-5c. The pressure coefficient along the center line (Fig. 5a) is in good agreement with other numerical and experimental results. Nevertheless, there is some discrepancy near the nose region. This may be due to the fact that the upstream solutions are based on the conical solutions. But, solutions match exactly with results from H-type grid, this is because grid topology near the center line is the same for both grid types. At 41.67% and 68.33% chordwise position, the

pressure ratios are plotted against the conical spanwise coordinates y/x tan (ϕ). They are in excellent agreement with experimental and numerical results (Fig. 5b and 5c). In addition they are much closer to the experimental results compared with results from H-type grid. This is due to good grid orthogonality in the case of O-type grid. On the thick sections near the nose the pressure is highest on the centerline and falls toward the leading edge. Figure 5d shows the cross-flow velocity at 5%, 23%, 41%, 59%, 77% and 95%.

Results for ten degrees angle of attack are compared with experimental results. The computed pressures are plotted in Figs. 6a-6d. At 17%, 30%, 50% and 70% chordwise position, the pressure ratios are plotted against the conical spanwise coordinates y/x tan (ϕ). They are in good agreement with experimental and numerical results (Fig. 6a-6d). On the thick sections near the nose the pressure is highest on the centerline and falls toward the leading edge whereas near the trailing edge the spanwise distribution is more 'wing like' with the maximum pressure at the leading edge. The changeover is shown by the pressure peaks in the pressure distributions at x/c=0.5 and 0.7 at 10° angle of attack. There are some discrepancy near x/c=30-50; this may be due to the fact that Squire 3 has not used the exact model of the Butler wing. In order to mount the model in the wind tunnel, the lower surface was distorted to include a sting support. Figure 6e shows the cross-velocity at 5%, 23%, 41%, 59%, 77% and 95%. These figures show a weak cross-wise separations at suction side which is confined to the body. At 59%, the cross flow has separated but a well defined vortex is not visible. Squire[9] has performed a series of tests to investigate the effects of thickness on the longitudinal characteristic of a delta wing of aspect ratio. The tests on the thick symmetrical delta wings have confirmed that the lift curve slope decreases as thickness is increased. This loss of lift is associated with a

weaker vortex system giving less nonlinear lift. Squire[3] also observed a pair vortices at the trailing edges, but there was no sign of any spanwise flow outboard of these vortices.

Concluding Remarks

General formulations are presented to investigate the flow field over complex configurations for high speed free stream conditions. An advanced algebraic method is used to generate grids around these configurations. The computational procedure developed is applied to investigate the flow field over a Butler wing. Illustrative results obtained for specified free stream conditions compare very well with available experimental and numerical results. Results are obtained only for laminar flow over a Butler wing at Mach number of 3.5, Reynolds number of 2x106/ft (6.56x106/m), free static temperature of 390°R (216.67°K), wall temperature of 1092°R (606.67°K), length of 0.80 ft (0.2438 m) and the wing is at zero and ten degree angles of attack. Two types of grid have been generated for this wing; H-type and O-type. Results of both cases are compared and discussed.

Acknowledgement

The authors would like to express their appreciation to Dr. Lars-Erik Eriksson of Old Dominion University for his helpful discussion on implementation of smoothing and Dr. R. W. Newsome of Air Force Wright Aeronautical Laboratories for his discussion on the conical solutions of Navier-Stokes equations. The first and third authors have been supported partially by NASA/Langley Research Center under NCCI-68.

REFERENCES

1. Butler, D. S., "The Numerical Solution Of Hyperbolic System Of Partial Differential Equations In Three Independent Variable," Proceedings Of The Royal Society, Series A,Mathematical And Physical Sciences, No. 1281, Vol. 255, April 1960, pp. 232-252.

2. Walkden, F. and Caine, P., "Surface Pressure on A Wing Moving With Supersonic Speed", Proceedings Of Royal Society Of London, Series A, Volume 341, 1974, pp. 177-193.

3. Squire, L. C., "Measured Pressure Distributions And Shock Shapes on a Simple Delta Wing,"The Aeronautical Quarterly",Volume 32, Part 3, August 1981, pp. 188-198.

4. Smith, R.E., "Two-Boundary Grid Generation for the Solution of the Three-Dimensional Compressible Navier-Stokes Equations," NASA Technical Memorandum 83123, May 1981.

5. MacCormack, R. W. and Baldwin, B.S., "A Numerical Method for Solving the Navier-Stokes Equations with Application to Shock-Boundary Layer Intersections," AIAA paper 75-1, AIAA 13th Aerospace Sciences Meeting, Pasadena, CA, January 20-22, 1975.

6. Newsome, R. W., Adams, M. S., "Numerical Simulation of Vortical-Flow Over an Elliptical-Body Missile at High Angle of Attack," AIAA Paper 86-0559, AIAA 24th Aerospace Sciences Meeting, Reno, Nevada, January 6-9, 1986.

7. Roache, P.J., Computational Fluid Dynamics, Hermosa Publisher, 1972.

8. Squire, L.C., "Measured Pressure Distribution and Shock Shapes on a Simple Delta Wing," Cambridge University, Department of Engineering, CUED/Aero/Tr9, 1979.

9. Squire, L.C., "Some Effects of Thickness on the Longitudinal Characteristic of the Sharp Edges of Delta Wings at Low Wings," The Aeronautical Journal of the Royal Aeronautical Society, Vol. 72, February 1968, pp. 151-155.

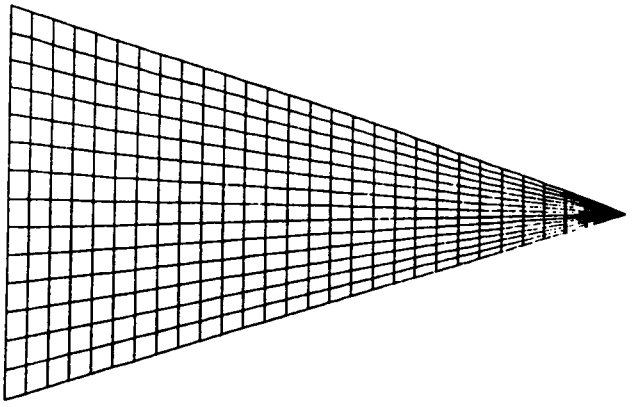

a. Top View

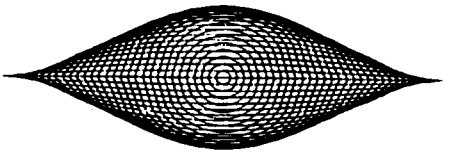

b. Front View

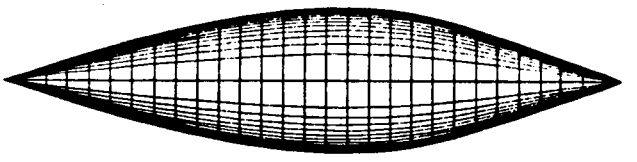

c. Side View

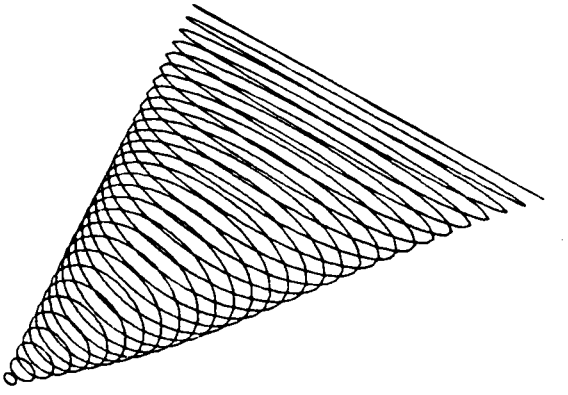

d. Oblique View

Figure 1. Physical Model of a Butler Wing

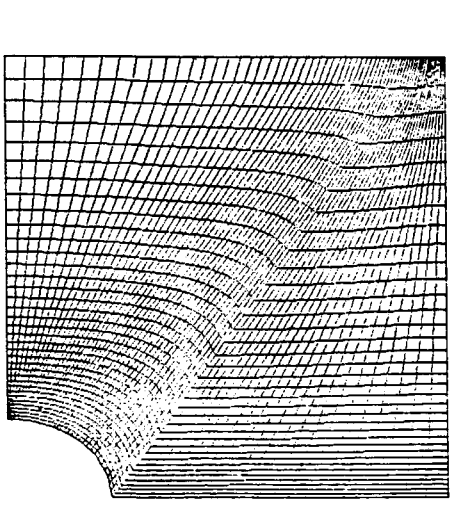

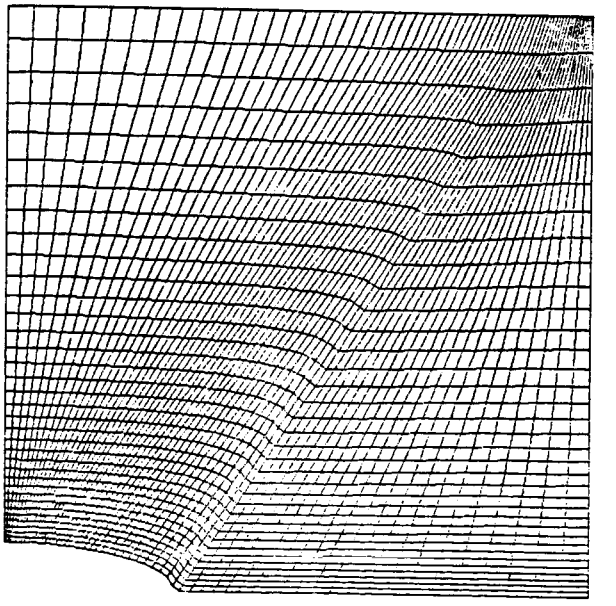

Figure 2. H-Type Grid for a Butler Wing

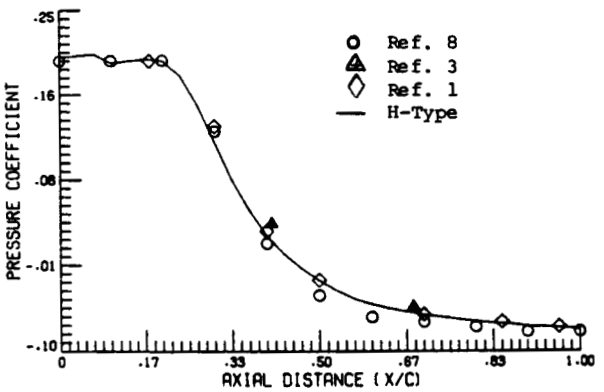

Figure 3a. Pressure Coefficient Along the Center Line

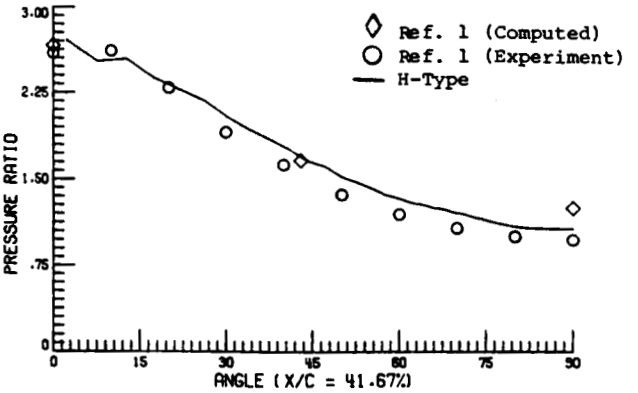

Figure 3b. Pressure Ratio at 41.67% of Chord

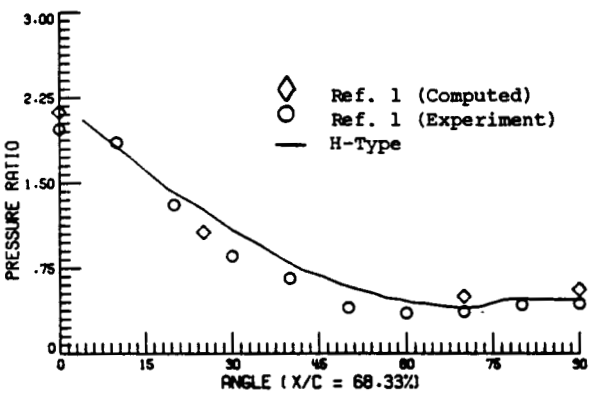

Figure 3c. Pressure Ratio at 68.33% of Chord

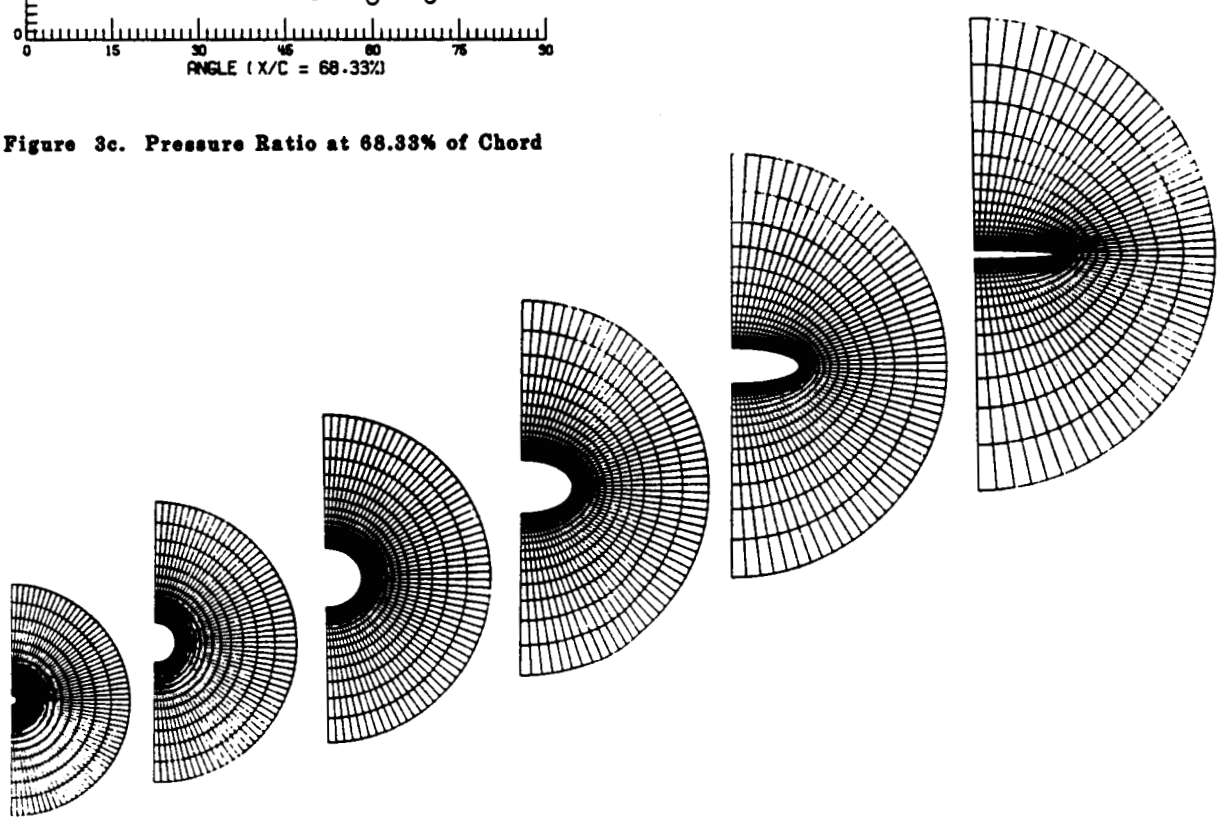

Figure 4. O-Type Grid for a Butler Wing

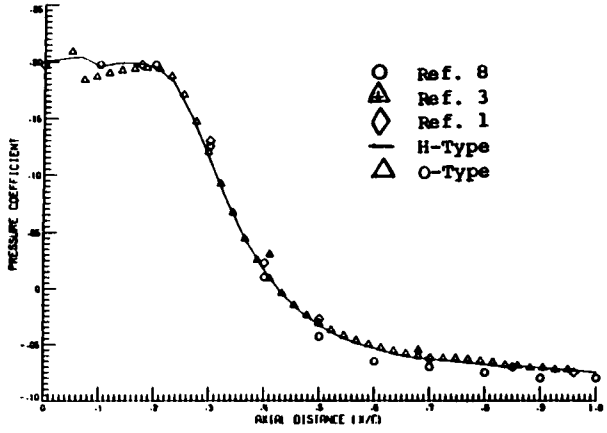

Figure 5a. Pressure Coefficient Along the Center Line

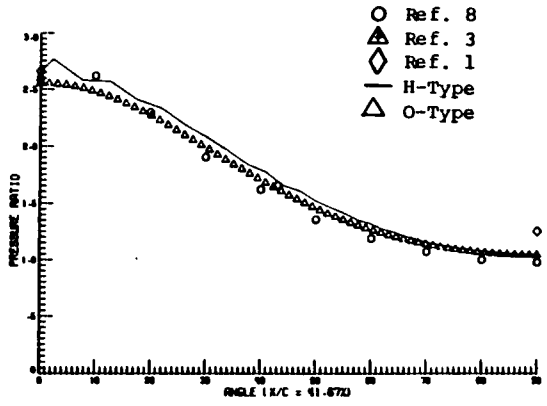

Figure 5b. Pressure Ratio at 41.67% of Chord

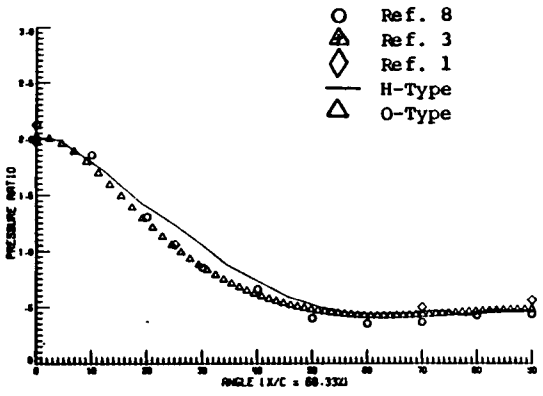

Figure 5c. Pressure Ratio at 88.33% of Chord

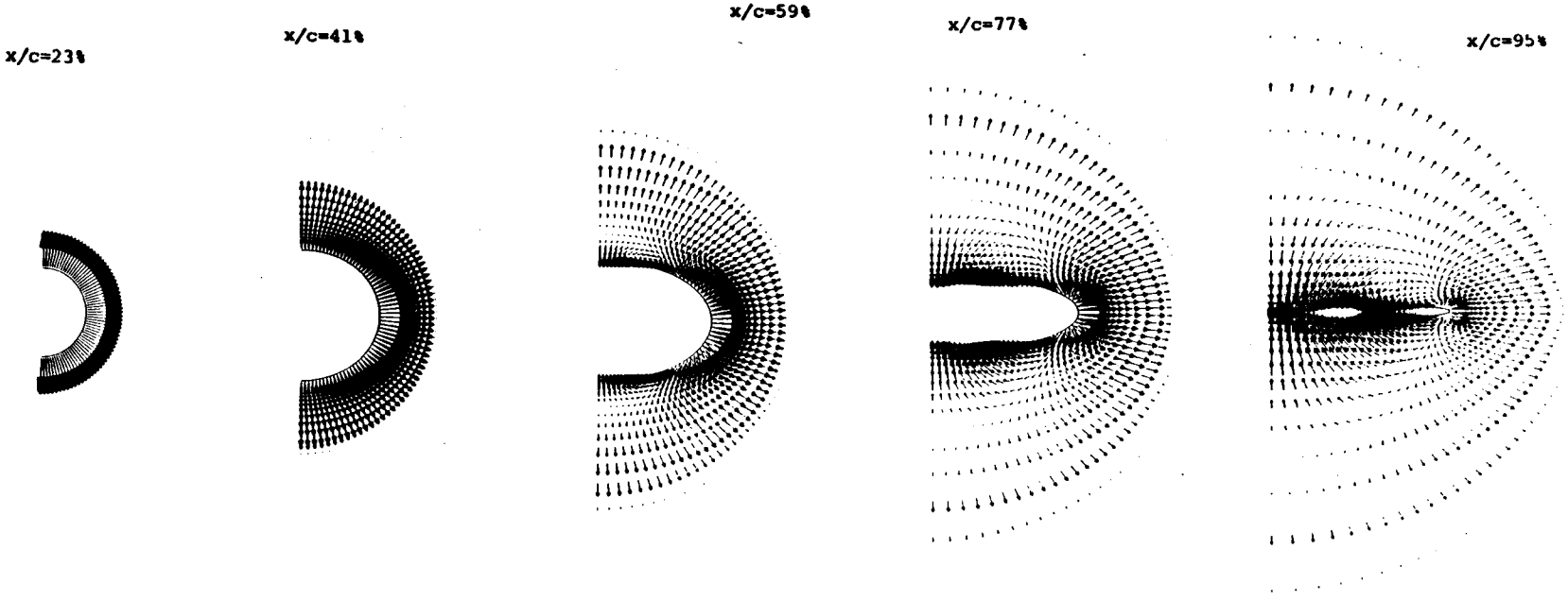

Figure 5d. Cross-flow velocity vectors (Zero Angle of Attack)

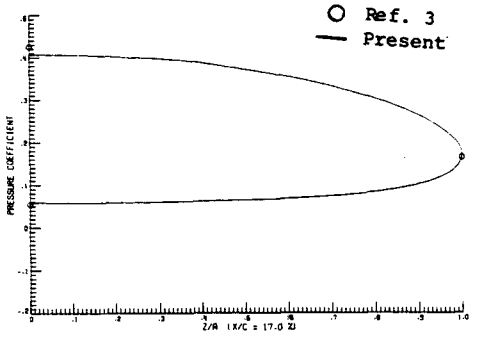

Figure 6a. Pressure Coeffient

(X/C 17% , Ten Degree Angle of Attack)

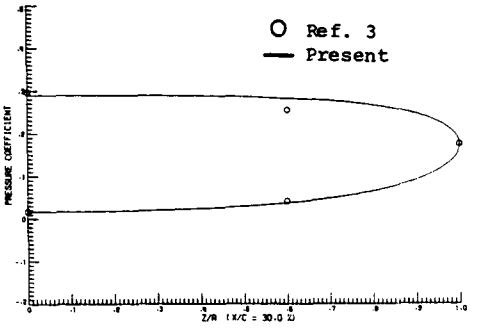

Figure 6b. Pressure Coeffient

(X/C 30% , Ten Degree Angle of Attack)

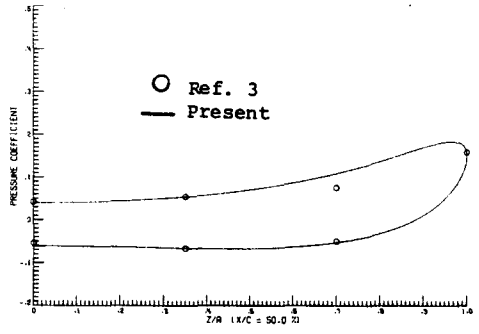

Figure 6c. Pressure Coeffient

(X/C 50% , Ten Degree Angle of Attack)

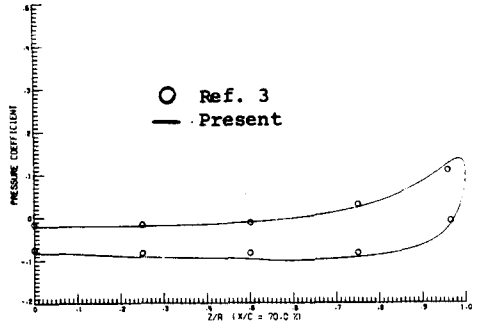

Figure 6d. Pressure Coeffient

(X/C 70% , Ten Degree Angle of Attack)

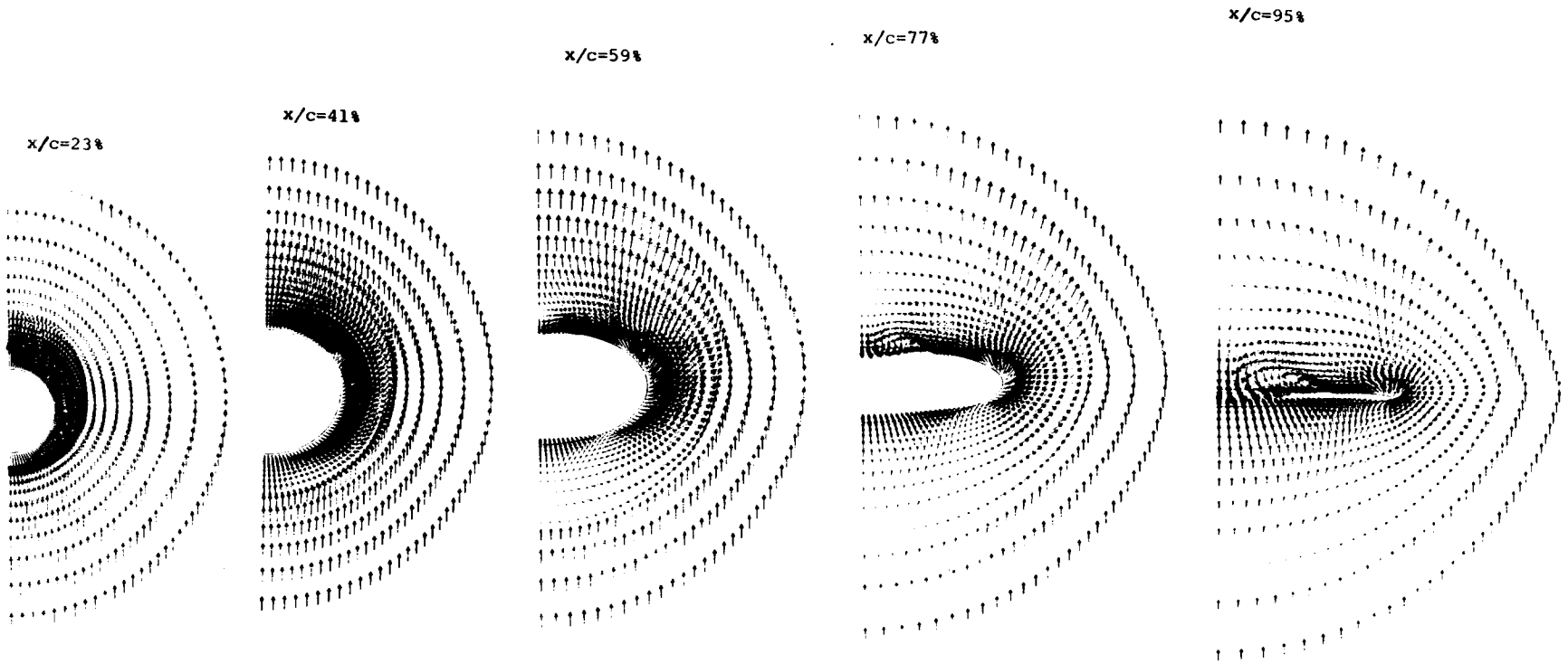

Figure 6e. Pressure Coeffient (X/C Ten Degree Angle of Attack)